ACS APPLIED MATERIALS & INTERFACES

Research Article

www.acsami.org

Templated Polymer Replica Nanoparticles to Facilitate Assessment of Material-Dependent Pharmacokinetics and Biodistribution

Danzi Song,[†] Jiwei Cui,[†,⊥] Huanli Sun,[†,▽] Tri-Hung Nguyen,[‡] Sheilajen Alcantara,[§] Robert De Rose,[§] Stephen J. Kent,[*,§,∥] Christopher J. H. Porter,[*,‡] and Frank Caruso[*,†]

[†]ARC Centre of Excellence in Convergent Bio-Nano Science and Technology, and the Department of Chemical Engineering, School of Chemical and Biomedical Engineering, The University of Melbourne, Parkville, Victoria 3010, Australia

[‡]ARC Centre of Excellence in Convergent Bio-Nano Science and Technology, and Drug Delivery Disposition and Dynamics, Monash Institute of Pharmaceutical Sciences, Monash University, Parkville 3052, Australia

[§]ARC Centre of Excellence in Convergent Bio-Nano Science and Technology, and the Department of Microbiology and Immunology, The University of Melbourne, at the Peter Doherty Institute for Infection and Immunity, Parkville, Victoria 3010, Australia

[∥]Melbourne Sexual Health Centre and Department of Infectious Diseases, Alfred Health, Central Clinical School, Monash University, Melbourne, Victoria 3800, Australia

Supporting Information

ABSTRACT: Surface modification is frequently used to tailor the interactions of nanoparticles with biological systems. In most cases, the chemical nature of the treatments employed to modify the biological interface (for example attachments of hydrophilic polymers or targeting groups) is the focus of attention. However, isolation of the fundamental effects of the materials employed to modify the interface are often confounded by secondary effects imparted by the underlying substrate. Herein, we demonstrate that polymer replica particles templated from degradable mesoporous silica provide a facile means to evaluate the impact of surface modification on the biological interactions of nanomaterials, independent of the substrate. Poly(ethylene glycol) (PEG), poly(*N*-(2 hydroxypropyl)methacrylamide) (PHPMA), and poly(methacrylic acid) (PMA) were templated onto mesoporous silica and cross-linked and the residual particles were removed. The resulting nanoparticles, comprising interfacial polymer alone, were then investigated using a range of in vitro and in vivo tests. As expected, the PEG particles showed the best stealth properties, and these trends were consistent in both in vitro and in vivo studies. PMA particles showed the highest cell association in cell lines in vitro and were rapidly taken up by monocytes in ex vivo whole blood, properties consistent with the very high in vivo clearance subsequently seen in rats. In contrast, PHPMA particles showed rapid association with both granulocytes and monocytes in ex vivo whole blood, even though in vivo clearance was less rapid than the PMA particles. Rat studies confirmed better systemic exposure for PEG and PHPMA particles when compared to PMA particles. This study provides a new avenue for investigating material-dependent biological behaviors of polymer particles, irrespective of the properties of the underlying core, and provides insights for the selection of polymer particles for future biological applications.

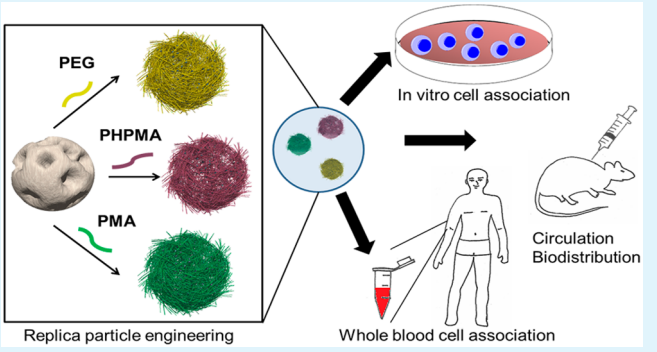

KEYWORDS: *nanoengineering, replica hydrogel particles, mesoporous silica particles, cell association, biodistribution*

INTRODUCTION

Nanoengineered particles have shown promise in biomedicine, particularly for diagnosis and treatment of diseases.[1−4] Polymer-based hydrogel particles are of particular interest in drug delivery as their physicochemical properties can be tailored by versatile fabrication methods for specific applications.[5,6] The influence of particle shape, size, and surface chemistry on bio−nano interactions has been extensively investigated.[7−9] Spherical structures are most commonly used and studied, and it has been shown that particles with sizes ranging from 20 to 200 nm have significant potential in targeted drug delivery applications that require long blood circulation times.[7] Chemical modifications that can modulate particle characteristics, such as hydrophilicity, surface charge, and immunogenicity, can greatly influence the fate of the particles in vivo. Hydrophilic materials, such as poly(ethylene glycol) (PEG) and poly(*N*-(2-hydroxypropyl)methacrylamide) (PHPMA), have shown high resistance to protein adsorption,

Received: August 4, 2017
Accepted: September 11, 2017

DOI: 10.1021/acsami.7b11579
ACS Appl. Mater. Interfaces XXXX, XXX, XXX−XXX

extended blood circulation, and improved plasma exposure of the drug vehicle in vivo.[10−12] These so-called "stealth" materials are frequently used for the modification of nanoparticles or proteins and as carriers of drugs and genes.[12−15]

Surface modification is widely used to modulate particle properties to influence cellular interactions, immune recognition, and other biological interactions in vitro and in vivo. The final properties achieved are highly dependent on various factors, including the degree of modification, chain molecular weight when polymers are used, and architecture of the modifying agent.[16−19] Depending on the surface modifications, the underlying particles can still influence the ensuing biological interactions. An alternative to surface modification is to engineer particles that are composed primarily of the material of interest. This can provide a systematic approach to compare material-dependent biological effects, as potential differences arising from surface modification are minimized. Furthermore, there are no particle cores that could interfere with the biological interactions.

Replica particles (RPs) prepared by mesoporous silica (MS) templating, a promising subset of polymer hydrogel particles, can be a valuable tool for investigating bio−nano interactions.[20] MS templating can accommodate diverse polymer types and facilitate the fabrication of particles with controlled material composition, size, and shape. To date, we have reported the generation of polymer particles by infiltrating polymers into the MS template pores via electrostatic attraction and subsequent cross-linking, followed by template removal.[21−23] However, the polymer infiltration step can take considerable time (up to 8 h) to allow for sufficient diffusion and loading of the polymer, especially for neutral polymers such as PEG.[18,24] Alternatively, particles can be obtained by surface-initiated polymerization of monomers in the MS particles.[25−29] However, there are very few reports on the synthesis of "stealthy" RPs. For instance, polymer−silica composite particles prepared from polymerization of itaconic acid and poly(ethylene glycol)methyl acrylate within MS particles without core removal were described.[27] The method required a rather lengthy period of light irradiation (7 h) in organic solvent in an inert reaction environment. Recently, we introduced a method to produce zwitterionic- and poly(oligo(ethylene glycol) methyl ether methacrylate)-based particles within MS particles.[28] However, the process required repeated freeze−pump−thaw cycles at an elevated temperature (50 °C). Furthermore, the use of low-molecular weight monomers in the preparation of PEG-based particles via surface-initiated polymerization, as described above, can lead to particle instability, especially in a complex biological environment in vivo.[30−33]

A recently developed templating approach termed atom transfer radical polymerization-mediated continuous assembly of polymers (CAP_{ATRP}) has been reported.[34,35] Herein, this method is presented, however, using high-molecular weight polymers (≥20 kDa) to prepare RPs and facilitate investigation of material-dependent biological behaviors in vitro, ex vivo, and in vivo. This approach enables facile assembly of previnyl-modified polymers (referred to as macrocross-linkers) under moderate reaction conditions (room temperature and water as solvent).[36,37] This method is amenable to diverse macrocross-linkers and has distinct advantages: (i) the formation of particles proceeds in a rapid one-pot reaction under moderate conditions while retaining the advantage of MS templating; (ii) cross-linking and the addition of functional groups or responsive linkers can be performed simultaneously to allow for multifunctionality and triggered degradation and release; (iii) the core material used for templating can be removed to prevent confounding biological interactions; and (iv) the size and shape of the template is conferred to the RPs, allowing for a high degree of control over variables important for biological interactions.

Three types of CAP_{ATRP} RPs, referred to as PEG, PHPMA, and poly(methacrylic acid) (PMA) particles thereafter, were fabricated using three macrocross-linkers: acrylated PEG (**P1**), acrylated PHPMA (**P2**), and methacrylate-functionalized PMA (PMA-AEMA; **P3**). PEG and PHPMA were chosen because they are the most widely used low-fouling and biocompatible synthetic polymers for drug delivery applications in clinical trials.[13,38] Although numerous types of PEG- and PHPMA-based polymer−drug conjugates have been reported,[39,40] direct comparisons of the effects of PEG- and PHPMA-based replica nanoparticles on biological interactions have not been reported. PMA has been extensively studied owing to its ease of modification; however, it usually requires modification with PEG for biological applications, owing to its high fouling properties.[21] Hence, it was selected as a control.

A variety of studies have investigated the use of in vitro tests to examine the association or uptake of nanoparticles by immune cell-derived cell lines in culture media and thereafter predict nanoparticle interactions with the immune system and nanoparticle distribution to reticuloendothelial system organs in vivo.[41,42] However, these tests do not fully represent the physiological interactions of particles with primary cells in the more complex environment of fresh blood. Hence, an emerging method that can measure nanoparticle association with multiple immune cell subsets in human whole blood has some advantages[18,43,44] and has been found to be a more relevant test than cell line-based assays for assessing the stealth properties of PEG particles.[18] How human blood interactions with particles compare to in vivo behavior in commonly studied rodent models for particles composed of other materials has yet to be confirmed. In the present study, we demonstrate the construction of polymer particles with controllable size and composition via CAP_{ATRP} and investigate their cell association in vitro and ex vivo. Finally, we investigate their behavior in vivo, compare the predictive qualities of the ex vivo tests, and discuss the effects of material properties on biological behavior.

EXPERIMENTAL SECTION

Materials. α-Bromoisobutyryl bromide, 2-aminoethyl methacrylate hydrochloride (AEMA), 4-(4,6-dimethoxy-1,3,5-triazin-2-yl)-4-methylmorpholinium chloride (DMTMM), di(ethylene glycol) diacrylate (DEGDAA, technical grade, 75%), *N*,*N*,*N*′,*N*′,*N*″-pentamethyldiethylenetriamine (PMDETA, 99%), copper(II) bromide ($CuBr_2$, 99%), ammonia (25%), (3-aminopropyl)triethoxysilane (APTES, 99%), pyridine (anhydrous, 99.8%), sodium ascorbate (NaAsc, ≥98%), propargylamine hydrochloride, hydrofluoric acid (HF, 48 wt %), ammonium fluoride (NH_4F), methacrylic acid (MA), Dulbecco's phosphate-buffered saline (DPBS), PBS tablets, cetyltrimethylammonium tosylate (CTAT), triethanolamine and tetraethyl orthosilicate (TEOS), and isopropyl alcohol were purchased from Sigma-Aldrich (Australia) and used as received. 8-Arm PEG acrylate (M_w = 20 kDa) was purchased from JenKem Technology USA Inc. (China). Poly(methacrylic acid) sodium salt (30% solution, M_w = 15 kDa) was purchased from Polysciences (U.S.A.). Alexa Fluor 488 azide (Alexa Fluor 488 5-carboxamido-(6-azidohexanyl)), bis-(triethylammonium salt), 5-isomer (AF488-azide)), Alexa Fluor 594 Wheat Germ Agglutinin (AF594-WGA), Hoechst 33342, heat-inactivated fetal bovine serum (FBS), RPMI 1640 medium with GlutaMAX supplement, and Zeba spin desalting column (40 kDa, 0.5

DOI: 10.1021/acsami.7b11579
ACS Appl. Mater. Interfaces XXXX, XXX, XXX−XXX

mL) were provided by Invitrogen (Australia). Paraformaldehyde (PFA, 4%) was obtained from Chem-Supply (Australia). 4-Azidosalicylic acid (ring-5-^{3}H) was purchased from American Radiolabeled Chemicals, Inc. (U.S.A.). Ultima Gold scintillation fluid and Soluene-350 tissue solubilizer were purchased from PerkinElmer, Inc. (U.S.A.). Saline was obtained from Baxter Healthcare Pty., Ltd. (Australia). DBL Heparin Sodium Injection BP was purchased from Hospira (Australia). The water used in all experiments was obtained from an inline Millipore RiOs/Origin system and had a resistivity greater than 18.2 MΩ cm. Linear acrylated PHPMA macrocross-linker **P2** (M_n = 31 500 g mol^{-1}, M_w = 49 100 g mol^{-1}, $Đ$ = 1.56, acrylate functionality = 10 mol %) was kindly provided by Edgar Wong following a reported method.[34]

Synthesis of MS Particles. MS particles were synthesized according to a previously reported method.[18] A mixture of CTAT (960 mg), triethanolamine (174 mg), and water (50 mL) was stirred at 80 °C for 1 h, followed by the addition of 7.8 mL of TEOS. The mixture was further stirred at 80 °C for 2 h. The particles were then washed with water and ethanol thrice, dried at 80 °C overnight, and calcined at 550 °C for 6 h.

Synthesis of Macrocross-Linker P3. PMA-AEMA was synthesized through reaction of PMA with AEMA in the presence of DMTMM. Briefly, DMTMM (469 mg, 1.70 mmol) and AEMA (153 mg, 0.92 mmol) were added to PMA (15 mL, 500 mg, 4.63 mmol −COOH) in PB buffer (50 mM, pH 7.2). The mixture was allowed to react for 24 h at room temperature (~21 °C). PMA-AEMA was purified by dialysis against water and lyophilized for 48 h. Yield: 88%, 485 mg; methacrylate functionality: 13 mol %.

MS Particle Surface Modification. To attach ATRP initiators to the MS particle surface, the latter was functionalized. A particle dispersion (20 mg mL^{-1}) in ethanol was first prepared by vortexing and sonicating for 10 min. Ammonia and APTES were then added to the particle suspension at a volume ratio of ethanol/ammonia/APTES = 50:2:1, and the resulting suspension was continuously mixed on a rotating tube holder overnight. Amino-functionalized MS particles were then washed with ethanol, water, and pyridine by centrifugation at 9000 *g* for 8 min. The particles were then dispersed in anhydrous pyridine (900 μL), followed by the addition of α-bromoisobutyryl bromide (100 μL). The particle suspension was mixed continuously on a rotating tube holder overnight before washing with ethanol twice and subsequently with water twice. The particles were stored in ethanol in the fridge (4 °C) prior to use.

Fabrication of Replica Particles. Macrocross-linker **P1** (5.6 mg), **P2** (3.4 mg), or **P3** (2.2 mg) was added to water (100 μL) to prepare the macrocross-linker solution. Then, a polymer solution (200 μL) was prepared by mixing the marcocross-linker solution (100 μL) with DEGDAA (95 μL, 33.1 mg mL^{-1}, in DMSO) and MA (5 μL, 40 mg mL^{-1}, in DMSO; Figure S1). The resulting solution was then added to the bromo-initiator-functionalized MS particles (2 mg) while vortexing. The particle suspension was thoroughly mixed and incubated on a rotating tube holder for 5 min. Subsequently, PMDETA (5.7 μL, 20.9 mg mL^{-1}, in water), NaAsc (5.7 μL, 159.9 mg mL^{-1}, in water), and $CuBr_2$ (5.7 μL, 9.0 mg mL^{-1}, in water) solutions were sequentially added to the particle mixture to start polymerization at room temperature (~21 °C) with constant mixing for 10 h. The vinyl group molar ratio of macrocross-linker/DEGDAA/MA was kept at 1:10:1. The number of moles of the vinyl groups in macrocross-linker **P1** was calculated based on the average molecular weight of 20 kDa, and that in macrocross-linkers **P2** and **P3** was calculated using eq 1:

$$n_{\text{vinyl}} = \frac{m}{M_0} f_{\text{vinyl}} \quad (1)$$

where n_{vinyl} is the number of moles of the vinyl groups, m is the mass of macrocross-linkers, M_0 is the average molecular weight of each repeating unit of the polymer, and f_{vinyl} is the (meth)acrylate functionality of the macrocross-linker. After polymerization, the polymer-grafted hybrid particles were isolated by centrifugation at 5000 *g* for 5 min and then thoroughly washed with DMSO/water (500 μL, 1:1 *v*/*v*) twice, water once, and PBS once. A sonication water bath was used to aid dispersion. To convert the −COOH groups into alkyne groups, DMTMM (250 μL, 2.0 mg mL^{-1}, in PBS) and propargylamine (250 μL, 0.7 mg mL^{-1}, in PBS) were added to the particles, and the reaction solution was mixed thoroughly and incubated overnight (Figure S2). After reaction, the alkyne-modified polymer particles were isolated by centrifugation (5000 *g*, 5 min) and subsequently washed with water.

Template Removal and Labeling. To remove the template, buffered HF solution (200 μL, pH 5, 5 M HF/13.3 M NH_4F = 1:2 (*v*/*v*)) was added to the particle suspension (~50 μL). *Caution! HF is highly toxic. Care should be taken when handling HF solution, and only small quantities should be prepared.* The resultant polymer RPs were washed thrice with water by centrifugation (7000 *g*, 7 min) and resuspended in water.

The particles were labeled with AF488-azide (2 μL, 1 mg mL^{-1}, in DMSO) or ^{3}H-azidosalicylic acid (2 μL, 1 μCi μL^{-1}, in ethanol) via the CuAAC reaction. NaAsc (100 μL, 4.4 mg mL^{-1}, in water) and copper sulfate (100 μL, 1.8 mg mL^{-1}, in water) were added, and the resulting suspension was incubated on a rotating tube holder overnight at room temperature (~21 °C). Unreacted AF488-azide or ^{3}H-azidosalicylic acid and copper catalyst were removed using a Zeba column as per the manufacturer's instructions.

In Vitro Cell Association and Imaging. HeLa, THP-1, and RAW 264.7 cells were routinely cultured in DMEM and RPMI and DMEM media with 10% (v/v) FBS at 37 °C in a 5% CO_2 humidified atmosphere. For the cell association studies, cells were plated in a 24-well plate (60 000 cells per well) in 500 μL of media. HeLa and RAW 264.7 cells were allowed to adhere overnight. Then, 1.2 × 10^7 AF488-labeled particles were incubated with the cells (particle-to-cell ratio was 200:1) for 24 h at 37 °C in 5% CO_2. After incubation, the THP-1 cells were washed with DPBS thrice via centrifugation (500 *g*, 5 min) and resuspended in DPBS for subsequent flow cytometry analysis. The HeLa and RAW 264.7 cells were gently washed twice with DPBS before trypsinization and further washed with DPBS once and then analyzed by flow cytometry and FlowJo software, version 9.9 (Tree Star; Figure S3).

For imaging, the RAW 264.7 cells were seeded into 8-well Lab-Tek I chambered cover glass slides (Thermo Fisher Scientific, Australia) at 60 000 cells per well and allowed to adhere overnight in 500 μL of media. Then, 1.2 × 10^7 AF488-labeled particles were added to each cell chamber and incubated for 24 h (37 °C, 5% CO_2). After incubation, the cells were gently washed with DPBS twice and fixed using 4% PFA (200 μL) for 10 min at room temperature (~21 °C) in the dark. The cell membrane was stained with AF594-WGA (200 μL, 5 μg mL^{-1}) at 4 °C in the dark for 5 min. The cell nucleus was stained at room temperature in the dark for 10 min with Hoechst 33354 (200 μL, 0.1 mg mL^{-1}). Images were taken in DPBS buffer (DeltaVision microscope).

Ex Vivo Whole Blood Cell Association. Whole blood from a healthy volunteer was collected into sodium heparin Vacuette tubes (Greiner Bio-One). Cell counts were obtained using a CELL-DYN Emerald analyzer (Abbott). Phenotyping of leukocytes was performed prior to particle incubation, where whole blood (100 μL) was incubated at 21 °C for 30 min with anti-CD45-V500 (BD Biosciences, clone HI30), anti-CD3-Alexa Fluor 700 (BD Biosciences, clone SP34−2), and anti-CD14-APC H7 (BD Biosciences, clone MϕP9). Whole blood samples were prewarmed to 37 °C or chilled on ice before incubating with Alexa Fluor 488-labeled particles (particle/leukocyte = 100:1) at 37 °C (5% CO_2) and on ice for 1 h in 5 mL polystyrene tubes (BD Biosciences). Erythrocytes were then lysed in 10 volumes of BD FACS Lysing Solution (BD Biosciences), followed by washing with PBS (4 mL, 500 *g*, 5 min). Cells were fixed with BD Stabilizing Fixative (BD Biosciences), and all events in the tube were acquired on a BDLSRFortessa (BD Biosciences). Particle−cell association was analyzed using a FlowJo software, version 9.9 (Tree Star; Figure S4). A CD45+ gate was used to distinguish leukocytes from contaminating erythrocytes. Granulocytes were identified as SSC^{hi}, T cells as CD3+ lymphocytes, and monocytes as CD14+.

Radiolabeling and Activity Determination. Approximately 3.5 × 10^{10} particles (24 mg) were labeled with ^{3}H-azidosalicylic acid (2 μL, 1 μCi μL^{-1} in ethanol) via CuAAC (Figure S2), and the activity of

DOI: 10.1021/acsami.7b11579
ACS Appl. Mater. Interfaces XXXX, XXX, XXX−XXX

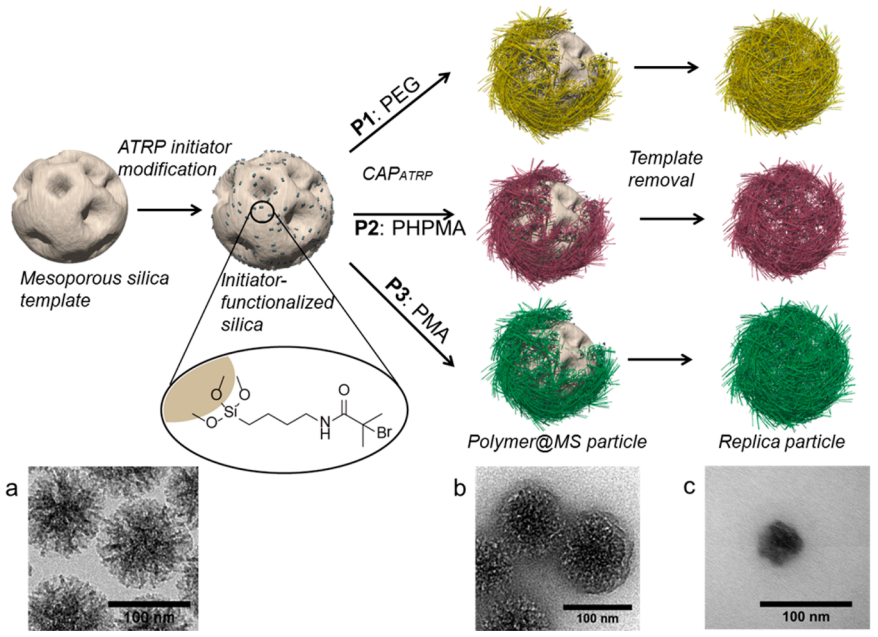

Figure 1. Fabrication of RPs from template surface modification to template removal. TEM images of (a) MS particles, (b) polymer-loaded MS particles (PEG@MS particles), and (c) PEG RP. The zeta potential values of the three RPs prepared were −8 ± 1 mV (PEG), −18 ± 2 mV (PHPMA), and −41 ± 2 mV (PMA), as measured in 5 mM phosphate buffer (pH 7.2).

the radiolabeled particles was measured by a Packard Tri-Carb 2000CA liquid scintillation counter (Meriden, CT). After removal of any unreacted radiolabel, by passing the particle suspension through a 40-kDa molecular weight cutoff Zeba Spin Desalting Column (Thermo Fisher Scientific, Australia) under centrifugation and less than 1% of the initial ^{3}H count was recorded in the wash supernatant (Figure S5), the particles were resuspended in heparinized saline (10 IU mL^{-1}) at approximately 0.6 μCi mL^{-1}. The specific activity of the particle suspension was determined by adding Ultima Gold scintillation fluid (2 mL) to aliquots of the radiolabeled particle solution (10 μL) in triplicate. Samples were well mixed, and the activity was measured by a liquid scintillation counter. The mean of triplicate values was used for subsequent calculations.

Intravenous Pharmacokinetic Studies. In vivo studies were conducted using male Sprague−Dawley rats (250−350 g; four rats per particle group) based on procedures previously described.[45] All animal studies were approved by the Monash Institute of Pharmaceutical Sciences Animal Ethics Committee (AEC number: MIPS.2014.22 (CHRIS PORTER)). Prior to administration, rats were anaesthetized under isoflurane, and the carotid artery and jugular vein were surgically cannulated using 0.96 mm × 0.58 mm polyethylene tubing (Microtube Extrusions, Australia). After the procedure, the rats were transferred to a metabolic cage to recover and fasted up to 14 h prior to and 8 h after dosing. Blank urine and predose blood (250 μL) were collected before dose administration. Each dose of RPs, equivalent to 0.6 μCi in 1 mL of heparinized saline, was administered as an infusion (1 mL min^{-1}) via the indwelling jugular cannula and then flushed with 250 μL of heparinized saline (10 IU mL^{-1}) to ensure any residual formulation was administered. Blood samples (250 μL) were subsequently collected from the carotid artery at 1, 2, 5, 10, 20, 40, 60, 120, 240, 480, and 1440 min after dose administration. Blood samples were transferred immediately into tubes containing heparin (10 μL, 1000 IU mL^{-1}), and the resulting heparinized blood was centrifuged at 500 *g* for 5 min to separate plasma. Heparinized saline was flushed through the cannula between samples to maintain patency of the cannula.[45] Duplicate aliquots (50 μL) of plasma samples were added to two 4 mL scintillation vials, and Ultima Gold scintillation fluid (2 mL) was added for scintillation measurements. The mean of the duplicate values was used for subsequent calculations. The results were expressed as either percentage of injected dose per rat by normalizing to the total plasma volume or microgram of RPs per milliliter of plasma. Total plasma volume was calculated based on the following equation: plasma volume (mL) = 0.55(0.06 body weight (g) + 0.77).[46]

Biodistribution Studies. In addition to the particles examined, free 4-azidosalicylic acid (ring-5-^{3}H) label at the same radioactivity (i.e., 0.6 μCi of ^{3}H per milliliter in heparinized saline) as the label was present in the RPs was administered to the rats to allow comparison with the biodistribution pattern of free label (3 rats). In all cases, after collection of the last plasma sample (24 h after IV administration), animals were humanely killed by injection of sodium pentobarbital (0.5 mL, Lethabarb, 60 mg of pentobarbitone sodium mL^{-1}) via the jugular cannula. The organs, lung, liver, spleen, heart, pancreas, kidney, and brain, were then removed by dissection, weighed, and stored at −20 °C until processed. Urine samples up to 24 h after dose administration were collected. Organ tissues were treated according to a previously reported protocol with slight modifications.[45] Organ tissues were added to water (5 mL) and homogenized in a gentleMACS dissociator (Miltenyi Biotech Australia Pty., Ltd., NSW, Australia) running a gentleMACS C tube RNA program for 5−10 s. Homogenized tissue samples were analyzed in two sets and with triplicates in each set. Each organ sample (equivalent of 100 mg of organ mass, based on wt % of organ contained) was placed in a 20 mL scintillation vial. One set of samples was untreated, whereas the other was spiked with radiolabel of known radioactivity (∼10 000 disintegrations per minute (dpm)) to provide organ counting efficiency data. The samples were solubilized in Soluene-350 (2 mL) and isopropyl alcohol (2 mL) and incubated at 60 °C overnight. Samples were then cooled to room temperature (∼21 °C) and bleached with 30% w/v hydrogen peroxide (200 μL) before the addition of Ultima Gold scintillation fluid (10 mL). Samples were well mixed and kept at 4 °C for 96 h in the dark without agitation before scintillation counting. Blank tissues from untreated rats were also processed as above to provide a background measurement. After the cooling period, 24 samples were measured at a time to avoid significant temperature fluctuation in the counter, which was set to 12 °C.

Blank urine and urine samples collected after dosing were placed in 50 mL preweighed tubes. Six aliquots of urine samples (200 μL) were divided into two sets (with triplicate in each set). One set was untreated, and the other was spiked with a radiolabel of known radioactivity (∼10 000 dpm) to determine counting efficiency. The urine sample was added to Ultima Gold scintillation fluid (2 mL) and well mixed before scintillation counting. Urine samples were then

DOI: 10.1021/acsami.7b11579
ACS Appl. Mater. Interfaces XXXX, XXX, XXX−XXX

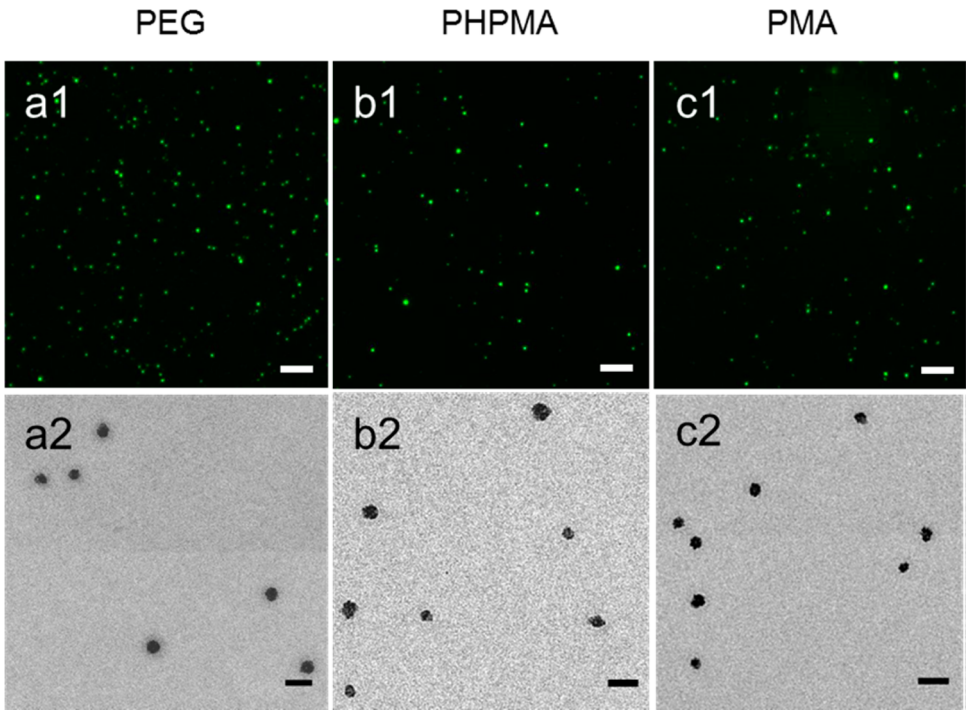

Figure 2. (a1−c1) Fluorescence microscopy and (a2−c2) TEM images of (a1, a2) PEG, (b1, b2) PHPMA, and (c1, c2) PMA RPs. Scale bars: 5 μm (a1−c1) and 100 nm (a2−c2).

measured by the Packard Tri-Carb 2000CA scintillation counter (Meriden, CT).

The acquired raw data of tissue and urine samples were used to calculate the efficiency of scintillation counting by the following equation:

$$\text{efficiency} = \frac{\text{spiked sample} - \text{sample}_{\text{uncorr}}}{\text{spike solution}} \quad (2)$$

where spiked sample is the radioactivity of the spiked sample (dpm), $\text{sample}_{\text{uncorr}}$ is the radioactivity measured in the untreated sample, and spike solution is the known quantity of radioactivity added to the spiked samples. The efficiency value was then used to correct each sample measurement due to the effect of quenching resulting from sample processing. The following formula applies:

$$\text{sample}_{\text{corr}} = \frac{\text{sample}_{\text{uncorr}}}{\text{efficiency}} \quad (3)$$

where $\text{sample}_{\text{corr}}$ is calculated to give the true activity value of the tissue sample (100 mg). The activity of whole organ and total urine collection were calculated based on the weight percentage of total organ mass and urine mass included within the measured samples. The biodistribution results were expressed as a percentage of injected dose in the whole organ or per gram of organ tissue.

Characterization. Fluorescence microscopy images of all of the RPs were acquired on an inverted Olympus IX71 microscope equipped with a UF1032 fluorescence filter cube and a 100× oil immersion objective (Olympus UPFL20/0.5NA, W.D1.6). Deconvolution microscopy images were obtained using a DeltaVision (Applied Precision) microscope equipped with a 60× 1.42 NA oil objective and a standard fluorescein isothiocyanate/tetramethylrhodamine/cyanine5 (FITC/TRITC/CY5) filter set. Transmission electron microscopy images were taken using a FEI Tecnai G2 Spirit instrument at an operating voltage of 120 kV. Scanning transmission electron microscopy images were obtained using a FEI Teneo Volumescope. Atomic force microscopy experiments were performed on a JPK NanoWizard II BioAFM. Typical scans were recorded in tapping mode using MikroMasch silicon cantilevers (NSC/CSC). The height of the RPs was determined using JPK SPM image processing software (version V.4.4.29). HeLa, THP-1, and RAW 264.7 cell association assays were performed on an Apogee A50-Microflow System at an excitation wavelength of 488 nm. At least 1.1×10^4 cells were counted, and samples were prepared in triplicate. Zeta potential and DLS measurements of the particles were conducted on a Malvern Zetasizer Nano ZS.

RESULTS AND DISCUSSION

For the preparation of polymer RPs, MS particles with an average diameter of 110 ± 10 nm were first synthesized and used as sacrificial templates (Figures S6 and 1a). MS particles were first amino-functionalized with (3-aminopropyl)-triethoxysilane (APTES) and then reacted with α-bromoisobutyryl bromide to introduce ATRP initiator on the particle surface. Macrocross-linker **P1**, **P2**, or **P3** was mixed with the cross-linker di(ethylene glycol) diacrylate (DEGDAA) and (meth)acrylic acid (MA) at an overall (meth)acrylate molar ratio of macrocross-linker/DEGDAA/MA = 1:10:0.8. After polymerization, the polymer-infiltrated MS particles (Figure 1b) were denser than the silica cores, suggesting successful formation of the polymer complex on and within the templates. Once the templates were removed, RPs with different macrocross-linkers as the main component were obtained with an average diameter of 50 ± 13 nm in the dry state (Figure 1c). The dimensions of the particles agreed with those measured in the scanning transmission electron microscopy (STEM) images (Figure S7). The particles could be well dispersed in both aqueous and organic solutions, and the hydrodynamic size of the particles in water measured by dynamic light scattering (DLS) was 160 ± 20 nm (Figure S8). This value corresponds to approximately 40% swelling relative to the diameter of the template regardless of polymer species. The similar swelling behavior may rely on the efficiency of polymerization of the vinyl groups and/or the molecular architecture of the cross-linkers. The different network structures may influence the porosity of the polymer particles

DOI: 10.1021/acsami.7b11579
ACS Appl. Mater. Interfaces XXXX, XXX, XXX−XXX

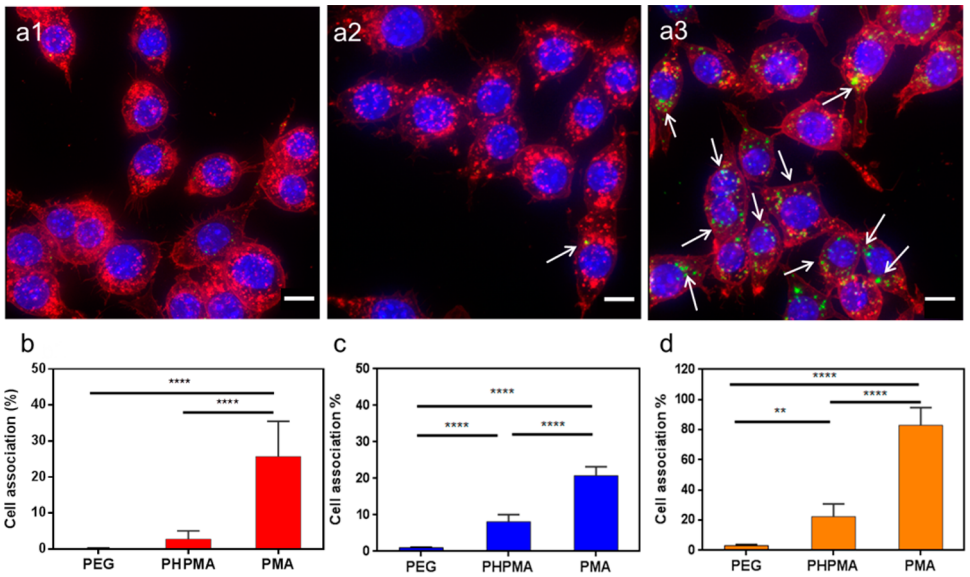

Figure 3. Deconvolution microscopy images of RAW 264.7 cells treated with AF488 fluorescently labeled CAP_{ATRP} RPs (a1) PEG, (a2) PHPMA, and (a3) PMA. RAW 264.7 cells were incubated with the particles (green, as indicated by the arrows) at a particle-to-cell ratio of 200:1 for 24 h at 37 °C. Cell membranes were stained with Alexa Fluor 594 Wheat Germ Agglutinin (AF594-WGA; red) and nuclei were stained with Hochest 33342 (blue). Scale bars are 5 μm. (b–d) Flow cytometry analysis of particles incubated with (b) HeLa, (c) THP-1, and (d) RAW 264.7 cells at a particle-to-cell ratio of 200:1 after 24 h incubation at 37 °C. At least 1.1×10^4 cells were counted per measurement. Values are mean ± standard deviation (SD; $n = 3$). One-way analysis of variance (ANOVA) significance shown as ** $p < 0.01$; **** $p < 0.0001$.

and therefore the permeability and cargo loadings. To enable fluorescence and radioactive labeling for the subsequent biological studies, the carboxylic acid groups of the particles were first converted into alkynes by reaction of the particles with propargylamine. Alexa Fluor 488 azide was then conjugated to the particles via copper(I)-catalyzed alkyne–azide cycloaddition (CuAAC) for fluorescence visualization.

The zeta potential values were similar to those measured before template removal and after alkyne modification. The small negative value for the PEG particles may be due to deprotonation of the unreacted carboxylic acid groups introduced for labeling. The thickness of the particle surface layer after air-drying was measured by atomic force microscopy (AFM; Figure S9). The results showed that among all of the RPs prepared, the PEG particles collapsed to the greatest extent (~10% of the hydrodynamic diameter), whereas the collapsed thickness of the PHPMA and PMA particles reduced to ~16% and ~61% of their original hydrodynamic diameter. Although it was difficult to measure the stiffness of particles directly, the degree of thickness reduction indicated that the PEG particles exhibited the softest property among all RPs studied. The TEM analysis also agreed with the shrinkage in particle size observed when the particles were dehydrated on the copper grid (Figure 2).

In Vitro Cell Association of Replica Particles. All three types of the RPs were separately incubated with the human cervical cancer cell line HeLa, human monocyte cell line THP-1, and murine macrophage cell line RAW 264.7 to study their interactions with commonly used cancer cells and phagocytic cells. At a particle-to-cell ratio of 200:1 and after incubation for 24 h at 37 °C, less than 0.5% and 3% of the HeLa cells were associated with the PEG and PHPMA particles, respectively. In contrast, the degree of association was significantly higher for the PMA particles (~25%). Association of the particles with THP-1 cells showed a similar trend: PEG (~1%) < PHPMA (~8%) < PMA (~21%). The degree of association of the RAW 264.7 cells with the PHPMA (~23%) and PMA (~83%) particles was higher when compared with that of the particles with the other two cell lines. However, PEG–RAW264.7 cell association remained low (<3%). Although all three types of particles were internalized by these macrophage cells to some extent (Figure 3a), the PEG particles consistently showed the lowest degree of association across all three cell lines, which is consistent with their stealth properties. Although the deconvolution images suggested almost negligible association of the PHPMA particles with RAW 264.7 cells, quantitative flow cytometry data suggested that they were less stealthy than the PEG particles but significantly better than the PMA particles. Studies have shown that softer particles tend to exhibit significantly reduced uptake by immune cells and cancer cells.[47,48] The stiffness of the particles, which varies in the order of PEG < PHPMA < PMA, may also reflect the trend of cell association observed herein. Surface chemistry is generally considered as another key factor that influences nonspecific interactions with biological environment. Typically, stronger hydration results in lower interactions with biological components due to large repulsive forces from the tightly bound water layer.[49,50] PEG and PHPMA are both highly hydrophilic materials, and PEG is more highly hydrated. Thus, PEG has been used to modify HPMA blocks to improve their hydrophilicity.[51] PMA is a negatively charged polymer and displays strong electrostatic interactions with proteins, which can potentially lead to the high cell association.

Ex Vivo Whole Blood Assay. We have recently shown that studying particle–cell interactions using freshly drawn human blood is a more sensitive approach than using basic cell line-based assays.[18] In that study, a particle-to-cell ratio of 100:1 was sufficient to make a comparison, and hence the same particle-to-cell ratio was used in the present study. Human blood contains multiple subsets of white blood cells, including phagocytic and nonphagocytic cells. Granulocytes and monocytes are the two major phagocytes responsible for eliminating

DOI: 10.1021/acsami.7b11579
ACS Appl. Mater. Interfaces XXXX, XXX, XXX–XXX

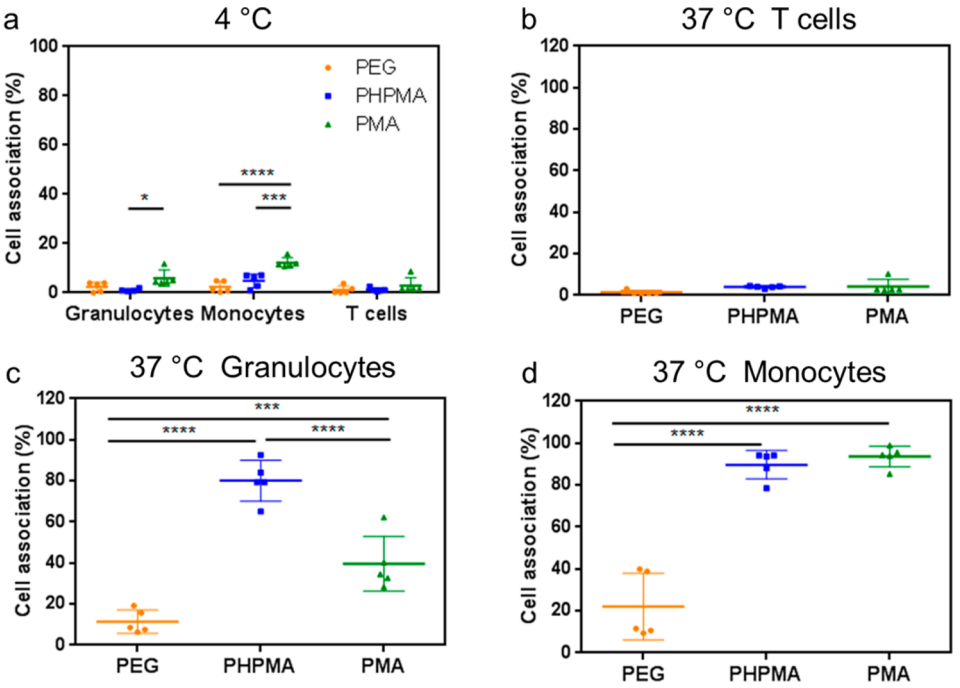

Figure 4. Association of PEG, PHPMA, or PMA particles with phagocytic (granulocytes and monocytes) and nonphagocytic cells (T cells) after incubation for 1 h in human whole blood: (a) association of the RPs in three cell populations at 4 °C; and association of the RPs with (b) T cells, (c) granulocytes, and (d) monocytes at 37 °C. Cell association was quantified by flow cytometry. Values are mean ± SD. One-way ANOVA significance shown as * $p < 0.05$; *** $p < 0.001$; **** $p < 0.0001$.

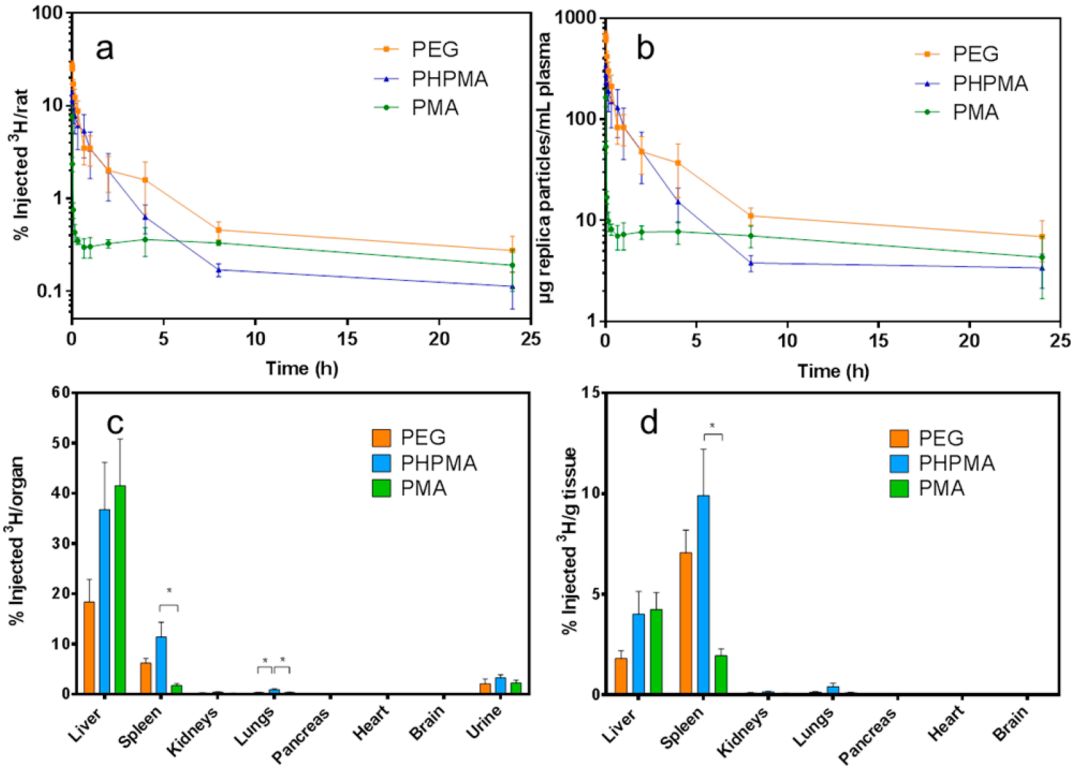

Figure 5. Pharmacokinetic and biodistribution data for RPs of different macrocross-linkers after intravenous administration to rats: (a) plasma concentration−time profile normalized to % injected ^{3}H per rat; (b) plasma concentration−time profile normalized to particles mass per milliliter of plasma; (c) percentage distribution of ^{3}H in organs after sacrifice at 24 h; and (d) percentage distribution of ^{3}H in organs after sacrifice at 24 h, normalized for tissue mass. Values are mean ± SD (n = 4 rats). One-way ANOVA significance shown as * $p < 0.05$.

foreign entities such as pathogens, waste, or debris in the blood and are expected to also indicate particle clearance by fixed macrophages in the liver and spleen.[52] High association with these cells reduces the number of particles available for delivery to the desired cell type or organ. The three types of RPs were incubated with human whole blood at a particle-to-cell ratio of

DOI: 10.1021/acsami.7b11579
ACS Appl. Mater. Interfaces XXXX, XXX, XXX−XXX

Table 1. Overview of Calculated Pharmacokinetic Parameters and Statistical Analysis

RPs	AUC_{0-t} (μg mL^{-1} h)	Cl (mL h^{-1})	V_D (mL)	$t_{1/2b}$ (h)
PMA	208.6 ± 58.2	121.7 ± 7.0	191.3 ± 24.8	
PHPMA	858.0 ± 345.9	32.7 ± 16.2	67.4 ± 26.4	2.1 ± 1.1
PEG	1252.7 ± 348.0	20.3 ± 6.0	36.3 ± 6.3	2.9 ± 0.7
significance comparison[a]				
PEG vs PHPMA	ns	ns	ns	ns
PEG vs PMA	** $p = 0.0071$	**** $p < 0.0001$	**** $p < 0.0001$	–
PHPMA vs PMA	ns	**** $p < 0.0001$	*** $p < 0.001$	–

[a]ns, nonsignificant; – , value could not be calculated because of fast particle clearance.

100:1 for 1 h at 4 °C and at 37 °C. Association with phagocytes (granulocytes and monocytes) and nonphagocytic cells (T cells) were investigated by flow cytometry. The assay was repeated five times with fresh blood from the same human donor (Figure 4). At 4 °C, at which active biological processes are either absent or at least very significantly reduced (and therefore where particle association is likely to primarily reflect surface association or adsorption and not uptake), the association of all particles with the blood cells was low, and subtle differences were observed. The PMA particles showed a higher degree of association with granulocytes (~6%) than the PHPMA particles (~1%), as well as a higher degree of monocyte association (~12%) than the PEG (~1%) and PHPMA (~5%) particles. At 37 °C, at which active uptake processes may occur and where association is expected to reflect both surface interaction and uptake, granulocyte association with PHPMA particles increased dramatically when compared with that with the PEG and PMA particles ($p < 0.0001$). This result suggests that energy-requiring processes, such as active transport processes, are responsible for the increase in interaction. The PHPMA particles also showed high monocyte association (~90%), although in this case, PMA particle association was also high. The interaction of the PHPMA and PMA particles with monocytes was 4-fold higher than that of the PEG particles ($p < 0.0001$). However, monocyte association of the PEG particles at that temperature (i.e., 37 °C) was higher than that observed at 4 °C, suggesting the potential for some cellular uptake even for PEG-based particles. There was negligible association with T cells at 4 and 37 °C for all three RPs studied, indicating a low level of nonspecific binding regardless of the material. As we have observed previously, the average association of PEG-based nanoparticles with monocytes was greater than that with granulocytes.[18,44] Similar results were observed for all three materials. Interestingly, the ex vivo results did not fully agree with the in vitro assay. Among all the RPs studied, PEG particles exhibited the lowest degree of association with all types of phagocytic cells in vitro and ex vivo. PMA particles exhibited the highest degree of association with monocytes in both assays. In contrast, the high degree of association of PHPMA particles with phagocytes, especially granulocytes in the whole blood environment, did not agree with the in vitro cell association data. Thus, additional studies were conducted to profile the in vivo behavior of the particles.

In Vivo Plasma Pharmacokinetics and Biodistribution of Replica Particles. In vivo studies in rats were conducted to provide further insight into the potential relationship between in vitro and ex vivo cell association studies and the in vivo pharmacokinetics and biodistribution patterns of the particles. Approximately 3.5×10^{10} (or 24 mg) of radiolabeled particles (equivalent to 0.6 μCi of ^{3}H) were administered to each rat intravenously, and blood samples were withdrawn at different time points until 24-h post injection.

The amount of dose remaining in plasma 24 h after administration was low for all three types of particles; that is, less than 1% of the initial dose (equivalent to ~10 μg of particles per milliliter of plasma; Figure 5a,b) was recorded. However, the plasma concentration of the PMA particles decreased the most rapidly; less than 1% of the initial dose remained in the plasma after 5 min. This result was consistent with the high degree of cell association in vitro and monocyte and granulocyte binding observed in the whole blood assay. Previous in vitro and ex vivo studies have also shown that PMA particles are effectively taken up by monocytes and macrophages, suggesting that they are strongly recognized by the immune system and cleared quickly.[18]

The plasma profiles of the PEG and PHPMA particles were similar (no statistically significant differences were evident in the area under the curve (AUC), clearance (Cl), volume of distribution (V_D), or terminal half-life ($t_{1/2b}$; Table 1)) and showed a slower decline than that observed for the PMA particles. The mean AUC of the PEG particles was ~0.5-fold higher than the mean value for the PHPMA particles and 6-fold higher than that of the PMA particles ($p < 0.01$), suggesting a lower degree of particle clearance. The V_D values also decreased in the order of PMA > PHPMA > PEG. However, owing to the relatively large variability in the observed AUC values between animals, no statistical significance between PEG and PHPMA was observed using a one-way ANOVA analysis. The PEG and PHPMA particles showed much lower Cl ($p < 0.0001$) and V_D ($p < 0.0001$ for PEG, $p < 0.001$ for PHPMA) than the PMA particles. The $t_{1/2b}$ of the PMA particles could not be accurately calculated owing to extremely rapid particle clearance. The $t_{1/2b}$ of the PEG particles (2.9 ± 0.7 h) was comparable with that of PHPMA (2.1 ± 1.1 h), reflecting proportional changes in Cl and V_D.

Contrary to the data presented here, a previously reported study using PEG- and PHPMA-modified liposomes (100 nm) showed that the systemic exposure (AUC) of PEGylated liposomes was more than double that of the PHPMA surface-modified liposomes after a single intravenous (IV) dose to mice.[53] In the present study, the examined PHPMA particles exhibited similar pharmacokinetics to the PEG particles, suggesting that both the "core" material used to prepare the particles and surface coating play a role in biological interactions. A previous report comparing PEG and PMA RPs, using an in vitro flow-based device containing extracellular matrix gel to predict in vivo circulation,[54] also showed rapid clearance of PMA particles, as consistent with the results presented herein.

As expected, the organ biodistribution patterns showed the largest accumulation of all three types of particles in the liver

DOI: 10.1021/acsami.7b11579
ACS Appl. Mater. Interfaces XXXX, XXX, XXX−XXX

Table 2. Overview of Calculated Organ and Urine Distribution (% Injected Dose per Organ or Total Urine)

RPs	liver	spleen	kidneys	lung	pancreas	heart	brain	urine
PMA	41.5 ± 16.1	1.8 ± 0.6	0.2 ± 0.2	0.3 ± 0.2	*c*	*c*	*c*	2.3 ± 0.8
PHPMA	36.8 ± 16.3	11.4 ± 5.1[a]	0.4 ± 0.2	0.8 ± 0.4[a]	*c*	*c*	*c*	3.3 ± 1.1
PEG	18.4 ± 7.8	6.2 ± 1.6	0.2 ± 0.1	0.3 ± 0.1[b]	0.1 ± 0.0	*c*	*c*	2.1 ± 1.4

[a]Statistically significantly different to PMA ($p < 0.05$). [b]Statistically significantly different to PHPMA ($p < 0.05$). [c]Identified below level of quantification.

Table 3. Overview of Calculated Organ and Urine Distribution (% Injected Dose per Gram Organ or per Gram Urine)

RPs	liver	spleen	kidneys	lung	pancreas	heart	brain	urine
PMA	4.2 ± 1.5	2.0 ± 0.6	0.1 ± 0.1	0.1 ± 0.0	*b*	*b*	*b*	0.6 ± 0.1
PHPMA	4.0 ± 1.9	9.9 ± 4.0[a]	0.2 ± 0.1	0.4 ± 0.3	*b*	*b*	*b*	0.8 ± 0.5
PEG	1.8 ± 0.7	7.1 ± 2.0	0.1 ± 0.0	0.1 ± 0.1	0.1 ± 0.0	*b*	*b*	0.4 ± 0.1

[a]Statistically significantly different to PMA ($p < 0.05$). [b]Identified below level of quantification.

and spleen (Figure 5c and Table 2). However, less than 20% of the PEG particles on average were found in the liver, and this value was lower than that measured for the PHPMA and PMA particles (37% and 42%, respectively) at 24-h post administration. A substantial amount of PHPMA particles accumulated in the spleen (~11.4%), which was significantly higher than that of the PMA particles (1.8%, $p < 0.05$). Pooling the data from the major organs of the mononuclear phagocyte system (MPS), approximately 25% of the dose of PEG particles, 48% of PHPMA particles, and 43% of PMA particles were recovered in the liver and spleen at 24 h. Particle accumulation in the MPS usually results in reduced circulation time owing to rapid phagocytosis in the liver and splenic filtration.[14] In general, the organ deposition patterns were consistent with the plasma clearance data; clearance of the PEG particles was slightly lower than that of PHPMA and much lower than of PMA. However, the similarity in liver and spleen uptake of the PHPMA and PMA particles did not reflect the fact that the residence time of the PHPMA particles in the bloodstream was significantly higher than that of the PMA particles. This observation underlines the complexities of interpreting kinetic differences in plasma concentration−time data based on terminal MPS distribution data. Thus, differences in plasma concentrations are clearly evident from 0 to 10 h post dose, and these differences are reflected in the large differences observed in plasma clearance. However, these differences are minimal at later time points when the terminal organ distributions were obtained. At 24-h post dose, the plasma levels (PEG > PMA > PHPMA) are, as expected, inversely proportion to MPS uptake where PHPMA > PMA > PEG.

To our knowledge, there is only one reported study on the pharmacokinetics and biodistribution of replica polymer particles with similar sizes made via MS templating method to those studied herein. In that study,[18] PEG-based particles were obtained by cross-linking terminal amine groups of PEG within a mesoporous template. These particles showed very different biodistribution patterns in mice,[18] and 110 nm-sized particles were almost evenly distributed in the liver, spleen, and lung and present at ~5% per gram organ tissue at 12-h post administration. In comparison, the PEG RPs employed in the present study showed lower uptake in the liver (1.8% dose g^{-1}), significantly lower uptake in the lung (0.1% dose g^{-1}), and slightly higher uptake by the spleen (7.1% dose g^{-1}). The different biodistribution patterns likely reflect the different sampling points (12 h vs 24 h herein) used and differences in particle stiffness and material composition stemming from the altered PEG particle fabrication method (surface-initiated polymerization vs infiltration and cross-linking) used. Studies have shown that softer particles can pass through physiological barriers more easily,[24,55,56] resulting in longer circulation time and different biodistribution properties.[47,55,56] The softer zwitterionic nanogels[56] showed lower splenic accumulation, whereas the softer PEG diacrylate hydrogel particles[47] and 2-hydroxyethyl acrylate hydrogels[55] accumulated in the spleen to a greater extent than their harder counterparts. This suggests that the stiffness of the particles not only influences the splenic uptake but is also highly material-dependent. In this study, the accumulation of the softer PHPMA RPs in the spleen was significantly higher than that of the PMA RPs. However, no further increases in uptake in the spleen were observed for the softest PEG RPs. This result confirmed the importance of evaluating the effect of the overall material which includes stiffness.

The accumulation levels of the PHPMA particles in the spleen (~9.9%) and lung (~0.8%) were slightly higher than those of the other two particle groups (lung $p < 0.05$, ~0.3% for both PEG and PMA particles; spleen $p < 0.05$ vs PMA particles). It has been shown that a significant fraction of the marginating granulocyte pool (MGP) distributes to the spleen (35%), liver (25%), and lungs (10%), and this accounts for 70% of the overall MGP.[57−59] The high accumulation of PHPMA particles in the spleen and lung might therefore reflect phagocytosis by granulocytes, as this was shown to be high based on the ex vivo blood incubation studies. Although biodistribution data have not been reported previously for PHPMA RPs, data pertaining to various PHPMA copolymer conjugates have been reported. Relatively large polymer molecular weights (>60 kDa) have shown patterns of conjugate accumulation in the spleen and lung,[38,60] as consistent with the findings here. In contrast, PHPMA-coated liposomes[53] have previously been shown not to accumulate in the spleen and lung after IV administration, suggesting again that the effects of surface coating materials on biodistribution may depend on the nature of the underlying particle. This core effect may be manifested by direct interaction of the core with the biological interface or via secondary effects on the orientation of the coating material. Studies have shown that PEGylation of polymer particles significantly enhances their accumulation in the spleen.[61,62] However, the PEG RPs did not show significantly higher splenic uptake when compared with the other two types of RPs studied herein, suggesting that the effect

DOI: 10.1021/acsami.7b11579
ACS Appl. Mater. Interfaces XXXX, XXX, XXX−XXX

of PEG coating may not represent the effect of the overall material.

After normalizing for organ mass (Figure 5d), the longer circulating PEG and PHPMA particles showed higher accumulation per gram of tissue in the spleen than in the liver, whereas PMA particles were predominantly captured by the liver (Table 3). Thus, high particle accumulation in the spleen alone does not necessarily contribute to the reduced circulation time but does influence the overall clearance if liver accumulation is also considerably high. However, for PEG- and PHPMA-coated liposomes, similar biodistributions in the liver (~20% dose) and spleen (~5% dose) were observed; additionally no significant difference in lung distribution was observed.[53]

There were minimal amounts of particles accumulated in the pancreas, heart, and brain for all three types of particles investigated (Table 2). Pooled urine, collected up to 24-h post administration, was also collected. Less than 4% of the initial dose for all of the particle types was detected in the urine. This value was significantly lower than the amount of free label recovered in the urine in the control study of the disposition of free label (Figure S10). Free label accumulation in the liver was also significantly lower than the particles (Figure S11). This suggests that the label was not released to any significant extent from the radiolabeled particles. The small amount of radiolabel present in the urine is likely derived from breakdown products due to hydrolysis of ester bonds of the macrocross-linkers in vivo.

In summary, the PEG particles showed the longest systemic circulation and the lowest overall MPS organ accumulation, as consistent with the predictions stemming from the in vitro and ex vivo cell association. The PHPMA particles shared similar pharmacokinetic properties to those of the PEG particles though they were more effectively captured by the spleen and lung possibly because of affinity to granulocytes. The PMA particles were cleared very rapidly. The data provide insight into the intrinsic effects of material properties on biological interactions, without conflicting effects of the underlying core material, and suggest that a consistent particle system such as the RPs may be favorable for examining material-dependent biological behaviors.

CONCLUSIONS

This study demonstrates the influence of polymer materials on cellular interactions, pharmacokinetics, and biodistribution. Polymer RPs (PEG, PHPMA, and PMA) with different macrocross-linker components were prepared via continuous assembly of polymers on MS templates. Monocyte and macrophage cell line-based in vitro assays and an ex vivo human whole blood assays were employed to evaluate cellular interaction and suggested in vitro that particle stealth properties were greatest for the PEG particles. Subsequent evaluation of the pharmacokinetics of all three types of particles in rats revealed that the PMA particles were rapidly eliminated from plasma and readily taken up by the liver. This result was consistent with the in vitro and ex vivo assays where PMA particles showed high monocyte and macrophage association. The PEG and PHPMA particles showed similar pharmacokinetic patterns but different biodistribution behaviors. The PEG particles displayed the lowest overall MPS accumulation, whereas the PHPMA particles appeared to accumulate in the spleen and lung, possibly owing to high association with granulocytes, as observed in the ex vivo blood incubation study. The accumulation levels of the PMA and PHPMA particles in MPS organs were similar and ~2-fold higher than that of the PEG particles. However, the circulation of the PHPMA particles was significantly longer than that of the PMA particles, at least at the early time points. Although there are very few studies on the in vivo properties of polymer template particles, comparison of the present results with data obtained with nanoparticles that have been surface-modified with polymers such as PEG, PHPMA, and PMA suggests that significant differences in biopharmaceutical behavior are possible. The reported modular templating approach therefore provides a means to obtain a read out of intrinsic biological interaction behavior, irrespective of the properties of the underlying core material. This approach may therefore be employed to provide an unbiased understanding of bio−nano interactions for a wider range of materials.

ASSOCIATED CONTENT

Supporting Information

The Supporting Information is available free of charge on the ACS Publications website at DOI: 10.1021/acsami.7b11579.

Molecular structure of 8-Arm-PEG acrylate, PHPMA acrylate, and PMA-AEMA, and the synthetic scheme of RPs; scheme of alkyne modification and ^{3}H labeling; flow cytometry gating strategies for in vitro and ex vivo data; radioactivity of RPs pre- and postradiolabeling; STEM images of PEG particles; DLS size distribution and AFM images of RPs; distribution of particles and free label in urine and organs. (PDF)

AUTHOR INFORMATION

Corresponding Authors

*E-mail: skent@unimelb.edu.au.
*E-mail: chris.porter@monash.edu.
*E-mail: fcaruso@unimelb.edu.au.

ORCID

Jiwei Cui: 0000-0003-1018-4336
Stephen J. Kent: 0000-0002-8539-4891
Frank Caruso: 0000-0002-0197-497X

Present Addresses

[⊥]Key Laboratory of Colloid and Interface Chemistry of Ministry of Education, and the School of Chemistry and Chemical Engineering, Shandong University, Jinan, Shandong 250100, China.
[▽]Biomedical Polymers Laboratory, and Jiangsu Key Laboratory of Advanced Functional Polymer Design and Application, College of Chemistry, Chemical Engineering and Materials Science, Soochow University, Suzhou 215123, China.

Author Contributions

The manuscript was written through contributions of all authors. All authors have given approval to the final version of the manuscript.

Notes

The authors declare no competing financial interest.

ACKNOWLEDGMENTS

This research was conducted and funded by the Australian Research Council (ARC) Centre of Excellence in Convergent Bio-Nano Science and Technology (Project No. CE140100036). This work was performed in part at the Materials Characterisation and Fabrication Platform (MCFP)

DOI: 10.1021/acsami.7b11579
ACS Appl. Mater. Interfaces XXXX, XXX, XXX−XXX

at The University of Melbourne and the Victorian Node of the Australian National Fabrication Facility (ANFF). We acknowledge Dr. Junling Guo and Dr. Ka Fung Noi (The University of Melbourne) for helpful discussions and Dr. Edgar H. H. Wong (University of New South Wales) for providing the PHPMA macrocross-linker.

REFERENCES

(1) Petros, R. A.; DeSimone, J. M. Strategies in the Design of Nanoparticles for Therapeutic Applications. *Nat. Rev. Drug Discovery* **2010**, *9*, 615−627.

(2) Xin, Y.; Huang, Q.; Tang, J. Q.; Hou, X. Y.; Zhang, P.; Zhang, L. Z.; Jiang, G. Nanoscale Drug Delivery for Targeted Chemotherapy. *Cancer Lett.* **2016**, *379*, 24−31.

(3) Wang, A. Z.; Langer, R.; Farokhzad, O. C. Nanoparticle Delivery of Cancer Drugs. *Annu. Rev. Med.* **2012**, *63*, 185−198.

(4) Banik, B. L.; Fattahi, P.; Brown, J. L. Polymeric Nanoparticles: the Future of Nanomedicine. *Wiley Interdiscip. Rev.: Nanomed. Nanobiotechnol.* **2016**, *8*, 271−299.

(5) De Koker, S.; Hoogenboom, R.; De Geest, B. G. Polymeric Multilayer Capsules for Drug Delivery. *Chem. Soc. Rev.* **2012**, *41*, 2867−2884.

(6) Kamaly, N.; Xiao, Z.; Valencia, P. M.; Radovic-Moreno, A. F.; Farokhzad, O. C. Targeted Polymeric Therapeutic Nanoparticles: Design, Development and Clinical Translation. *Chem. Soc. Rev.* **2012**, *41*, 2971−3010.

(7) Elsabahy, M.; Wooley, K. L. Design of Polymeric Nanoparticles for Biomedical Delivery Applications. *Chem. Soc. Rev.* **2012**, *41*, 2545−2561.

(8) Albanese, A.; Tang, P. S.; Chan, W. C. The Effect of Nanoparticle Size, Shape, and Surface Chemistry on Biological Systems. *Annu. Rev. Biomed. Eng.* **2012**, *14*, 1−16.

(9) Cui, J.; Richardson, J. J.; Björnmalm, M.; Faria, M.; Caruso, F. Nanoengineered Templated Polymer Particles: Navigating the Biological Realm. *Acc. Chem. Res.* **2016**, *49*, 1139−1148.

(10) Lääne, A.; Aaviksaar, A.; Haga, M.; Chytrý, V.; Kopeček, J. Preparation of Polymer-Modified Enzymes of Prolonged Circulation Times. Poly[*N*-(2-hydroxypropyl) Methacrylamide]-Bound Acetylcholinesterase. *Makromol. Chem.* **1985**, *9*, 35−42.

(11) Yang, J.; Kopeček, J. Macromolecular Therapeutics. *J. Controlled Release* **2014**, *190*, 288−303.

(12) Whiteman, K. R.; Subr, V.; Ulbrich, K.; Torchilin, V. P. Poly(HPMA)-Coated Liposomes Demonstrate Prolonged Circulation in Mice. *J. Liposome Res.* **2001**, *11*, 153−164.

(13) Kopeček, J.; Kopečková, P. HPMA Copolymers: Origins, Early Developments, Present, and Future. *Adv. Drug Delivery Rev.* **2010**, *62*, 122−149.

(14) Alexis, F.; Pridgen, E.; Molnar, L. K.; Farokhzad, O. C. Factors Affecting the Clearance and Biodistribution of Polymeric Nanoparticles. *Mol. Pharmaceutics* **2008**, *5*, 505−515.

(15) Oupický, D.; Howard, K. A.; Koňák, Č.; Dash, P. R.; Ulbrich, K.; Seymour, L. W. Steric Stabilization of Poly-l-Lysine/DNA Complexes by the Covalent Attachment of Semitelechelic Poly[*N*-(2-Hydroxypropyl)methacrylamide]. *Bioconjugate Chem.* **2000**, *11* (4), 492.

(16) Perry, J. L.; Reuter, K. G.; Kai, M. P.; Herlihy, K. P.; Jones, S. W.; Luft, J. C.; Napier, M.; Bear, J. E.; DeSimone, J. M. PEGylated PRINT Nanoparticles: the Impact of PEG Density on Protein Binding, Macrophage Association, Biodistribution, and Pharmacokinetics. *Nano Lett.* **2012**, *12*, 5304−5310.

(17) Yang, Q.; Jones, S. W.; Parker, C. L.; Zamboni, W. C.; Bear, J. E.; Lai, S. K. Evading Immune Cell Uptake and Clearance Requires PEG Grafting at Densities Substantially Exceeding the Minimum for Brush Conformation. *Mol. Pharmaceutics* **2014**, *11*, 1250−1258.

(18) Cui, J.; De Rose, R.; Alt, K.; Alcantara, S.; Paterson, B. M.; Liang, K.; Hu, M.; Richardson, J. J.; Yan, Y.; Jeffery, C. M.; Price, R. I.; Peter, K.; Hagemeyer, C. E.; Donnelly, P. S.; Kent, S. J.; Caruso, F. Engineering Poly(ethylene glycol) Particles for Improved Biodistribution. *ACS Nano* **2015**, *9*, 1571−1580.

(19) Venkataraman, S.; Ong, W. L.; Ong, Z. Y.; Loo, S. C. J.; Ee, P. L. R.; Yang, Y. Y. The Role of PEG Architecture and Molecular Weight in the Gene Transfection Performance of PEGylated Poly-(Dimethylaminoethyl Methacrylate) Based Cationic Polymers. *Biomaterials* **2011**, *32*, 2369−2378.

(20) Björnmalm, M.; Cui, J.; Bertleff-Zieschang, N.; Song, D.; Faria, M.; Rahim, M. A.; Caruso, F. Nanoengineering Particles Through Template Assembly. *Chem. Mater.* **2017**, *29*, 289−306.

(21) De Koker, S.; Cui, J.; Vanparijs, N.; Albertazzi, L.; Grooten, J.; Caruso, F.; De Geest, B. G. Engineering Polymer Hydrogel Nanoparticles for Lymph Node-Targeted Delivery. *Angew. Chem., Int. Ed.* **2016**, *55*, 1334−1339.

(22) Cui, J.; De Rose, R.; Best, J. P.; Johnston, A. P. R.; Alcantara, S.; Liang, K.; Such, G. K.; Kent, S. J.; Caruso, F. Mechanically Tunable, Self-Adjuvanting Nanoengineered Polypeptide Particles. *Adv. Mater.* **2013**, *25*, 3468−3472.

(23) Suma, T.; Cui, J.; Müllner, M.; Fu, S.; Tran, J.; Noi, K. F.; Ju, Y.; Caruso, F. Modulated Fragmentation of Proapoptotic Peptide Nanoparticles Regulates Cytotoxicity. *J. Am. Chem. Soc.* **2017**, *139*, 4009−4018.

(24) Cui, J.; Björnmalm, M.; Liang, K.; Xu, C.; Best, J.; Zhang, X.; Caruso, F. Super-Soft Hydrogel Particles with Tunable Elasticity in a Microfluidic Blood Capillary Model. *Adv. Mater.* **2014**, *26*, 7295−7299.

(25) Pasetto, P.; Blas, H.; Audouin, F.; Boissière, C.; Sanchez, C.; Save, M.; Charleux, B. Mechanistic Insight into Surface-Initiated Polymerization of Methyl Methacrylate and Styrene via ATRP from Ordered Mesoporous Silica Particles. *Macromolecules* **2009**, *42*, 5983−5995.

(26) Banerjee, S.; Paira, T. K.; Kotal, A.; Mandal, T. K. Surface-Confined Atom Transfer Radical Polymerization from Sacrificial Mesoporous Silica Nanospheres for Preparing Mesoporous Polymer/Carbon Nanospheres with Faithful Shape Replication: Functional Mesoporous Materials. *Adv. Funct. Mater.* **2012**, *22*, 4751−4762.

(27) Huang, L.; Liu, M.; Mao, L.; Xu, D.; Wan, Q.; Zeng, G.; Shi, Y.; Wen, Y.; Zhang, X.; Wei, Y. Preparation and Controlled Drug Delivery Applications of Mesoporous Silica Polymer Nanocomposites Through the Visible Light Induced Surface-Initiated ATRP. *Appl. Surf. Sci.* **2017**, *412*, 571−577.

(28) Müllner, M.; Cui, J.; Noi, K. F.; Gunawan, S. T.; Caruso, F. Surface-Initiated Polymerization within Mesoporous Silica Spheres for the Modular Design of Charge-Neutral Polymer Particles. *Langmuir* **2014**, *30*, 6286−6293.

(29) Zhou, H.; Wang, X.; Tang, J.; Yang, Y. W. Tuning the Growth, Crosslinking, and Gating Effect of Disulfide-Containing PGMAs on the Surfaces of Mesoporous Silica Nanoparticles For Redox/pH Dual-Controlled Cargo Release. *Polym. Chem.* **2016**, *7*, 2171−2179.

(30) Gref, R.; Lück, M.; Quellec, P.; Marchand, M.; Dellacherie, E.; Harnisch, S.; Blunk, T.; Müller, R. H. 'Stealth' Corona-Core Nanoparticles Surface Modified by Polyethylene Glycol (PEG): Influences of the Corona (PEG Chain Length and Surface Density) and of the Core Composition on Phagocytic Uptake and Plasma Protein Adsorption. *Colloids Surf., B* **2000**, *18*, 301−313.

(31) Fang, C.; Shi, B.; Pei, Y.-Y.; Hong, M.-H.; Wu, J.; Chen, H.-Z. In Vivo Tumor Targeting of Tumor Necrosis Factor-α-Loaded Stealth Nanoparticles: Effect of MePEG Molecular Weight and Particle Size. *Eur. J. Pharm. Sci.* **2006**, *27*, 27−36.

(32) Gillies, E. R.; Dy, E.; Fréchet, J. M. J.; Szoka, F. C. Biological Evaluation of Polyester Dendrimer: Poly(ethylene oxide) "Bow-Tie" Hybrids with Tunable Molecular Weight and Architecture. *Mol. Pharmaceutics* **2005**, *2*, 129−138.

(33) Seymour, L. W.; Miyamoto, Y.; Maeda, H.; Brereton, M.; Strohalm, J.; Ulbrich, K.; Duncan, R. Influence of Molecular Weight on Passive Tumour Accumulation of A Soluble Macromolecular Drug Carrier. *Eur. J. Cancer* **1995**, *31*, 766−770.

(34) Wong, E. H. H.; van Koeverden, M. P.; Nam, E.; Guntari, S. N.; Wibowo, S. H.; Blencowe, A.; Caruso, F.; Qiao, G. G. Assembly of

DOI: 10.1021/acsami.7b11579
ACS Appl. Mater. Interfaces XXXX, XXX, XXX−XXX

Nanostructured Films with Hydrophobic Subcompartments via Continuous Assembly of Polymers. *Macromolecules* **2013**, *46*, 7789−7796.
(35) Sun, H.; Cui, J.; Ju, Y.; Chen, X.; Wong, E. H. H.; Tran, J.; Qiao, G. G.; Caruso, F. Tuning the Properties of Polymer Capsules for Cellular Interactions. *Bioconjugate Chem.* **2017**, *28*, 1859−1866.
(36) Mertz, D.; Ochs, C. J.; Zhu, Z.; Lee, L.; Guntari, S. N.; Such, G. K.; Goh, T. K.; Connal, L. A.; Blencowe, A.; Qiao, G. G.; Caruso, F. ATRP-Mediated Continuous Assembly of Polymers for the Preparation of Nanoscale Films. *Chem. Commun.* **2011**, *47*, 12601−12603.
(37) Sun, H.; Wong, E. H. H.; Yan, Y.; Cui, J.; Dai, Q.; Guo, J.; Qiao, G. G.; Caruso, F. The Role of Capsule Stiffness on Cellular Processing. *Chem. Sci.* **2015**, *6*, 3505−3514.
(38) Lammers, T.; Subr, V.; Ulbrich, K.; Hennink, W. E.; Storm, G.; Kiessling, F. Polymeric Nanomedicines for Image-Guided Drug Delivery and Tumor-Targeted Combination Therapy. *Nano Today* **2010**, *5*, 197−212.
(39) Ulbrich, K.; Holá, K.; Šubr, V.; Bakandritsos, A.; Tuček, J.; Zbořil, R. Targeted Drug Delivery with Polymers and Magnetic Nanoparticles: Covalent and Noncovalent Approaches, Release Control, and Clinical Studies. *Chem. Rev.* **2016**, *116*, 5338−5431.
(40) Larson, N.; Ghandehari, H. Polymeric Conjugates for Drug Delivery. *Chem. Mater.* **2012**, *24*, 840−853.
(41) Dobrovolskaia, M. A.; Aggarwal, P.; Hall, J. B.; McNeil, S. E. Preclinical Studies To Understand Nanoparticle Interaction with the Immune System and Its Potential Effects on Nanoparticle Biodistribution. *Mol. Pharmaceutics* **2008**, *5*, 487−495.
(42) Lunov, O.; Syrovets, T.; Loos, C.; Beil, J.; Delacher, M.; Tron, K.; Nienhaus, G. U.; Musyanovych, A.; Mailänder, V.; Landfester, K.; Simmet, T. Differential Uptake of Functionalized Polystyrene Nanoparticles by Human Macrophages and a Monocytic Cell Line. *ACS Nano* **2011**, *5*, 1657−1669.
(43) Baumann, D.; Hofmann, D.; Nullmeier, S.; Panther, P.; Dietze, C.; Musyanovych, A.; Ritz, S.; Landfester, K.; Mailänder, V. Complex Encounters: Nanoparticles in Whole Blood and Their Uptake into Different Types of White Blood Cells. *Nanomedicine* **2013**, *8*, 699−713.
(44) Mann, S. K.; Dufour, A.; Glass, J. J.; De Rose, R.; Kent, S. J.; Such, G. K.; Johnston, A. P. R. Tuning the Properties of PH Responsive Nanoparticles to Control Cellular Interactions In Vitro and Ex Vivo. *Polym. Chem.* **2016**, *7*, 6015−6024.
(45) Boyd, B. J.; Kaminskas, L. M.; Karellas, P.; Krippner, G.; Lessene, R.; Porter, C. J. H. Cationic Poly-l-lysine Dendrimers: Pharmacokinetics, Biodistribution, and Evidence for Metabolism and Bioresorption after Intravenous Administration to Rats. *Mol. Pharmaceutics* **2006**, *3*, 614−627.
(46) Lee, H.; Blaufox, M. Blood Volume in The Rat. *J. Nucl. Med.* **1985**, *26*, 72−76.
(47) Anselmo, A. C.; Zhang, M.; Kumar, S.; Vogus, D. R.; Menegatti, S.; Helgeson, M. E.; Mitragotri, S. Elasticity of Nanoparticles Influences Their Blood Circulation, Phagocytosis, Endocytosis, and Targeting. *ACS Nano* **2015**, *9*, 3169−3177.
(48) Hartmann, R.; Weidenbach, M.; Neubauer, M.; Fery, A.; Parak, W. J. Stiffness-Dependent In Vitro Uptake and Lysosomal Acidification of Colloidal Particles. *Angew. Chem., Int. Ed.* **2015**, *54*, 1365−1368.
(49) Cao, Z.; Jiang, S. Super-Hydrophilic Zwitterionic Poly(carboxybetaine) and Amphiphilic Non-Ionic Poly(ethylene glycol) for Stealth Nanoparticles. *Nano Today* **2012**, *7*, 404−413.
(50) Singh, J.; Desai, S.; Yadav, S.; Narasimhan, B.; Kaur, H. Polymer Drug Conjugates: Recent Advancements in Various Diseases. *Curr. Pharm. Des.* **2016**, *22*, 2821−2843.
(51) Allmeroth, M.; Moderegger, D.; Gündel, D.; Buchholz, H.-G.; Mohr, N.; Koynov, K.; Rösch, F.; Thews, O.; Zentel, R. PEGylation of HPMA-Based Block Copolymers Enhances Tumor Accumulation In Vivo: A Quantitative Study Using Radiolabeling and Positron Emission Tomography. *J. Controlled Release* **2013**, *172*, 77−85.
(52) Dale, D. C.; Boxer, L.; Liles, W. C. The Phagocytes: Neutrophils and Monocytes. *Blood* **2008**, *112*, 935−945.
(53) Kierstead, P. H.; Okochi, H.; Venditto, V. J.; Chuong, T. C.; Kivimae, S.; Fréchet, J. M. J.; Szoka, F. C. The Effect of Polymer Backbone Chemistry on the Induction of the Accelerated Blood Clearance in Polymer Modified Liposomes. *J. Controlled Release* **2015**, *213*, 1−9.
(54) Braunger, J. A.; Bjornmalm, M.; Isles, N. A.; Cui, J.; Henderson, T. M. A.; O'Connor, A. J.; Caruso, F. Interactions Between Circulating Nanoengineered Polymer Particles and Extracellular Matrix Components in vitro. *Biomater. Sci.* **2017**, *5*, 267−273.
(55) Merkel, T. J.; Jones, S. W.; Herlihy, K. P.; Kersey, F. R.; Shields, A. R.; Napier, M.; Luft, J. C.; Wu, H.; Zamboni, W. C.; Wang, A. Z.; Bear, J. E.; DeSimone, J. M. Using Mechanobiological Mimicry of Red Blood Cells to Extend Circulation Times of Hydrogel Microparticles. *Proc. Natl. Acad. Sci. U. S. A.* **2011**, *108*, 586−591.
(56) Zhang, L.; Cao, Z.; Li, Y.; Ella-Menye, J.-R.; Bai, T.; Jiang, S. Softer Zwitterionic Nanogels for Longer Circulation and Lower Splenic Accumulation. *ACS Nano* **2012**, *6*, 6681−6686.
(57) Peters, A. M.; Saverymuttu, S. H.; Bell, R. N.; Lavender, J. P. Quantification of the Distribution of the Marginating Granulocyte Pool in Man. *Scand. J. Haematol.* **1985**, *34*, 111−120.
(58) Peters, A. M.; Saverymuttu, S. H.; Keshavarzian, A.; Bell, R. N.; Lavender, J. P. Splenic Pooling of Granulocytes. *Clin. Sci.* **1985**, *68*, 283−289.
(59) Peters, A. M.; Allsop, P.; Stuttle, A. W. J.; Arnot, R. N.; Gwilliam, M.; Hall, G. M. Granulocyte Margination in the Human Lung and Its Response to Strenuous Exercise. *Clin. Sci.* **1992**, *82*, 237−244.
(60) Wang, Y.; Ye, F.; Jeong, E. K.; Sun, Y.; Parker, D. L.; Lu, Z. R. Noninvasive Visualization of Pharmacokinetics, Biodistribution and Tumor Targeting of Poly[*N*-(2-hydroxypropyl)methacrylamide] in Mice Using Contrast Enhanced MRI. *Pharm. Res.* **2007**, *24*, 1208−1216.
(61) Peracchia, M. T.; Fattal, E.; Desmaële, D.; Besnard, M.; Noël, J. P.; Gomis, J. M.; Appel, M.; d'Angelo, J.; Couvreur, P. Stealth® PEGylated Polycyanoacrylate Nanoparticles for Intravenous Administration and Splenic Targeting. *J. Controlled Release* **1999**, *60*, 121−128.
(62) Bazile, D.; Prud'homme, C.; Bassoullet, M. T.; Marlard, M.; Spenlehauer, G.; Veillard, M. Stealth Me. PEG-PLA Nanoparticles Avoid Uptake by the Mononuclear Phagocytes System. *J. Pharm. Sci.* **1995**, *84*, 493−498.

DOI: 10.1021/acsami.7b11579
ACS Appl. Mater. Interfaces XXXX, XXX, XXX−XXX